Review of Scientific Instruments

# Fluid dynamic design and experimental study of an aspirated temperature measurement platform used in climate observation

Cite as: Rev. Sci. Instrum. **87**, 084503 (2016); https://doi.org/10.1063/1.4961645
Submitted: 02 June 2016 . Accepted: 13 August 2016 . Published Online: 29 August 2016

Jie Yang, Qingquan Liu, Wei Dai, and Renhui Ding





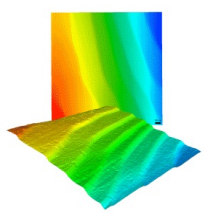
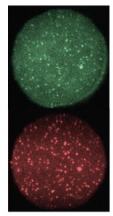





AIP Publishing

# Fluid dynamic design and experimental study of an aspirated temperature measurement platform used in climate observation

Jie Yang,[1,2,a)] Qingquan Liu,[3,4] Wei Dai,[2] and Renhui Ding[5]
[1]*Key Laboratory for Aerosol-Cloud-Precipitation of China Meteorological Administration, Nanjing 210044, China*
[2]*School of Atmospheric Physics, Nanjing University of Information Science and Technology, Nanjing 210044, China*
[3]*Jiangsu Key Laboratory of Meteorological Observation and Information Processing, Nanjing 210044, China*
[4]*Jiangsu Collaborative Innovation Center on Atmospheric Environment and Equipment Technology, Nanjing 210044, China*
[5]*Jiangsu Meteorological Observation Center, Nanjing 210008, China*

(Received 2 June 2016; accepted 13 August 2016; published online 29 August 2016)

Due to the solar radiation effect, current air temperature sensors inside a thermometer screen or radiation shield may produce measurement errors that are 0.8 °C or higher. To improve the observation accuracy, an aspirated temperature measurement platform is designed. A computational fluid dynamics (CFD) method is implemented to analyze and calculate the radiation error of the aspirated temperature measurement platform under various environmental conditions. Then, a radiation error correction equation is obtained by fitting the CFD results using a genetic algorithm (GA) method. In order to verify the performance of the temperature sensor, the aspirated temperature measurement platform, temperature sensors with a naturally ventilated radiation shield, and a thermometer screen are characterized in the same environment to conduct the intercomparison. The average radiation errors of the sensors in the naturally ventilated radiation shield and the thermometer screen are 0.44 °C and 0.25 °C, respectively. In contrast, the radiation error of the aspirated temperature measurement platform is as low as 0.05 °C. This aspirated temperature sensor allows the radiation error to be reduced by approximately 88.6% compared to the naturally ventilated radiation shield, and allows the error to be reduced by a percentage of approximately 80% compared to the thermometer screen. The mean absolute error and root mean square error between the correction equation and experimental results are 0.032 °C and 0.036 °C, respectively, which demonstrates the accuracy of the CFD and GA methods proposed in this research.  [http://dx.doi.org/10.1063/1.4961645]

## I. INTRODUCTION

Surface air temperature is the basic information of weather forecasting and climate change forecasting. In recent years, a series of researches have been focused on the air temperature.[1–4] Dillon suggested that the temperature data, in the period between 1961 and 2009, of 3186 weather stations across the world show 0.4 °C and 0.95 °C atmospheric temperature increases in tropical and northern hemisphere areas, respectively.[5] Haines reached a conclusion that through analyzing the data of satellite observation and researching the data from the weather stations, surface air temperature increased 0.09 °C and 0.17 °C every ten years, respectively.[6] In conclusion, the magnitude of air temperature change is in the order of 0.1 °C/10a. In order to observe the global, large scale, and local climate change accurately, the measurement accuracy of the air temperature observation system should be on the order of or less than 0.01 °C.

The radiation error is the dominant error source of the temperature measurement. To minimize the influence of solar radiation, temperature sensor needs to be housed in the radiation shield or the thermometer screen, which shades the instrument. However, the reflectivity of the thermometer screen and the radiation shield is incapable of reaching 100%, so they can still generate radiation heating significantly, which causes the airflow into the internal being heated, and then produces measurement error. In addition, the structures of thermometer screen and radiation shield are not conducive to air circulation, which reduces the response speed of the inner sensor. Due to these factors, the air temperature sensors inside the thermometer screen and the radiation shield affected by solar radiation could cause a measurement error of 0.8 °C or higher.[7,8] The airflow,[9] radiative regime,[10,11] and different coatings[12] have displayed remarkable impacts on the energy balance of radiation shields, which may lead to 2–8 °C errors in air temperature measurements under weak winds of ≤1 m/s and high solar irradiance of ≥800 W/m$^2$.[13–16] During daytime, the radiation error of a naturally ventilated radiation shield may reach 4.5–5 °C.[17] Low wind speed and high solar radiation intensity usually create a worst case scenario in terms of temperature observation accuracy.

A number of studies have investigated the performance of the shield, including field and wind tunnel tests.[12,18–23] The

a)Author to whom correspondence should be addressed. Electronic mail: yangjie396768@163.com

 

main finding from these studies is that the air temperature errors of radiation shield would range from −0.5 to 2.5 °C. Quayle found that the maximum-minimum temperature system (MMTS) averagely produces maximum temperatures roughly 0.4 °C lower and the minimum temperatures about 0.3 °C higher than the cotton region shelter (CRS).[24]

It is a generally accepted conclusion that a high performance radiation shield needs to be mechanically aspirated, while radiation errors are inversely proportional to the airflow velocity through the shield. When the wind speed is below 2 m/s and the radiation intensity is above 700 W/m$^2$, the air temperature errors were quite large (>2 °C).[25] The range of airflow velocity of model 43502 aspirated radiation shield is 5–11 m/s. When the wind speed and solar radiation intensity are 11 m/s and 1000 W/m$^2$, respectively, the radiation error of model 43502 aspirated radiation shield is 0.2 °C, which hardly meets the demand of high precision observation. It is assumed in this paper that a high power fan is necessary to achieve higher airflow velocity, if a radiation error of 0.1 °C or even lower is desired.

The computational fluid dynamics (CFD) technology is widely applied.[26,27] Some progress has been made to model the energy balance of naturally ventilated shield for the goal of correcting the radiation error.[14,16] Kurzeja proposed an approach, based on temperature sensors with different diameters, to estimate the radiation error.[28] Richardson modelled the airflow through the shields by using a general purpose software package Fluent to attain the airflow profile inside a Gill shield.[29] These models are relatively simple, and the simulation results can only offer airflow velocity and direction inside the shields. However, because of the limited level of maturity, the CFD technologies in 1990s and early 2000s were unable to construct a heat transfer model of radiation shield or thermometer screen. As a result, the numerical results of the temperature distribution and radiation errors in a thermometer screen and a radiation shield were unable to be obtained.

In this article, an aspirated temperature measurement platform is proposed. By using the method of CFD, the radiation error of the aspirated temperature measurement platform is solved, and the radiation error correction equation is obtained by fitting the CFD results using a genetic algorithm (GA) method, which may further improve the measurement accuracy of the aspirated temperature measurement platform.

## II. DESIGN OF THE ASPIRATED TEMPERATURE MEASUREMENT PLATFORM

### A. Computational fluid dynamics model

The aspirated temperature measurement platform consists of a platinum resistance sensor probe, an L-shaped radiation shield, a stepping motor, a centrifugal fan, and a temperature measurement module with a high accuracy thermometer circuit. To ensure a high surface reflection coefficient, the silver plating technique is applied to the L-shaped shield (Fig. 1).

The upper part of the shield can horizontally rotate under the control of a software. If the airflow-inlet of the shield and the airflow direction are unparallel, the air heated by the external shield wall may flow into the shield, thus increasing the measuring error. In addition, if the airflow-inlet of the shield and the airflow direction are parallel, the airflow velocity inside the shield may rise to its maximum value, thus decreasing the measuring error. The stepping motor can

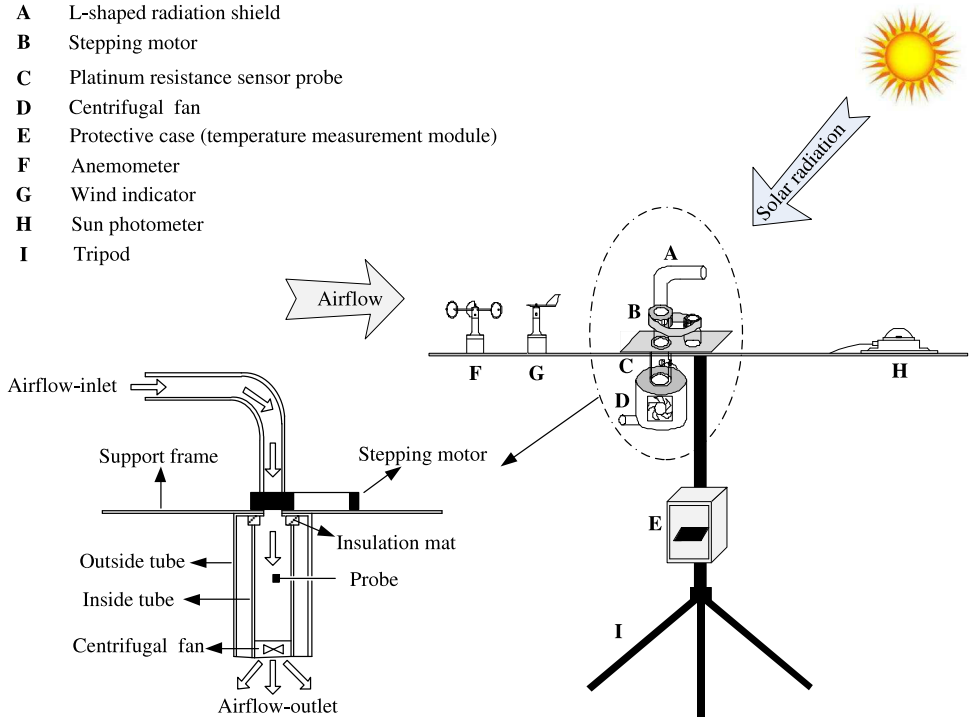


FIG. 1. Schematic of the aspirated temperature measurement platform.

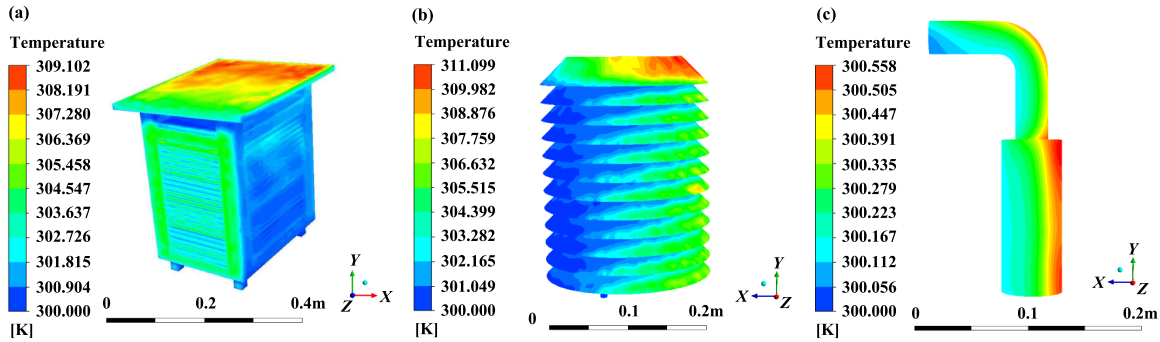


FIG. 2. Simulation result of the temperature fields. (a) Thermometer screen, (b) naturally ventilated radiation shield, and (c) aspirated temperature measurement platform.

rotate the airflow-inlet of the shield horizontally according to the wind direction to realize the alignment of airflow-inlet of the shield and the airflow direction. The lower part of the shield has a twin tube structure. An inside tube is protected and covered by an outside tube. Because the double-wall structure features relatively low thermal conductivity, the heat from the outside tube may be prevented from heating the temperature sensor probe in the inside tube, thus reducing the heat pollution. The centrifugal fan is installed at the bottom of the shield and sucks the air from top to bottom. The probe is installed in the center of the double tube of the shield. The temperature measurement module is placed inside the protective case.

Although large size of air domain is beneficial to improve the numerical solution accuracy, it also leads to computation complexity. It is concluded that the reasonable air domain size is 300 mm × 300 mm × 500 mm by comparing models with a variety of air domains. In order to obtain an ideal mesh, a grid software ICEM CFD is used to mesh the calculation model. The technology of unstructured mesh is adopted to generate a tetrahedral mesh. As the tetrahedral grids exist in the non-boundary area, the pentahedral prism grid is adopted near the boundary layer. The max size of mesh in the global area is 10 mm. A standard k-epsilon model and a SIMPLE algorithm are employed in the numerical computation. The density and thermal conductivity of the L-shaped shield are 8030 kg/m$^3$ and 16.27 W/(m K), respectively.

## B. Modeling of temperature field

In order to obtain the radiation errors of the aspirated temperature measurement platform, the temperature sensor in the naturally ventilated radiation shield, and the temperature sensor in the thermometer screen, the CFD models of these instruments are analyzed in identical environments. The ambient wind speed and solar radiation intensity are 2 m/s and 1000 W/m$^2$, respectively. The aspirated airflow velocity of the aspirated temperature measurement platform is 8 m/s. The reflectivity of the naturally ventilated radiation shield, the thermometer screen, and the L-shaped shield is 87%, 87%, and 92%, respectively. The temperature fields are shown in Fig. 2.

The simulation result of the aspirated temperature measurement platform shows that the radiation error of the probe is 0.041 °C (Fig. 2(c)). The radiation errors of the probes inside the thermometer screen and the naturally ventilated radiation shield are 0.352 °C and 0.526 °C, respectively (Figs. 2(a) and 2(b)). It can be seen that the thermometer screen and the naturally ventilated radiation shield have difficulty to meet the present air temperature measurement accuracy requirements, while the aspirated temperature measurement platform may improve the observation precision.

## C. Correction of radiation error

In order to obtain a universal correction equation of radiation error of the aspirated temperature measurement platform, the CFD method is applied to calculate the radiation errors of the aspirated temperature measurement platform at the condition of various solar radiation intensities and altitudes. The range of solar radiation intensity is 100–1200 W/m$^2$, and the altitude ranges from 0 to 5 km (Fig. 3).

The radiation error diminishes with increasing altitude and increases with increasing solar radiation. The largest radiation error is 0.09 °C, when the solar radiation intensity and altitude are 1200 W/m$^2$ and 5 km, respectively. The smallest radiation error is 0.004 °C, when the solar radiation intensity and altitude are 100 W/m$^2$ and 0 km, respectively. In order to obtain the correction equation of radiation error, the GA method is applied to fit the CFD results.

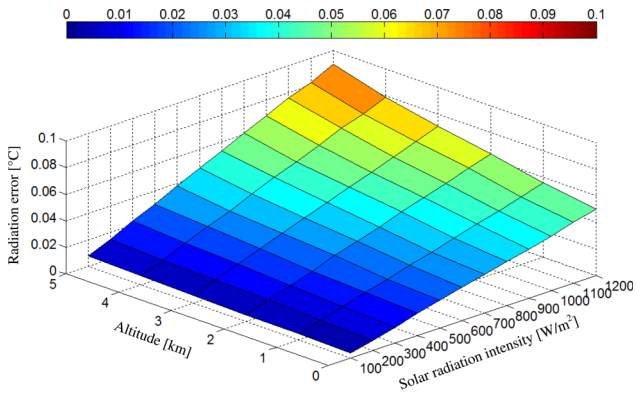


FIG. 3. Relationship among solar radiation intensity, altitude, and radiation error.

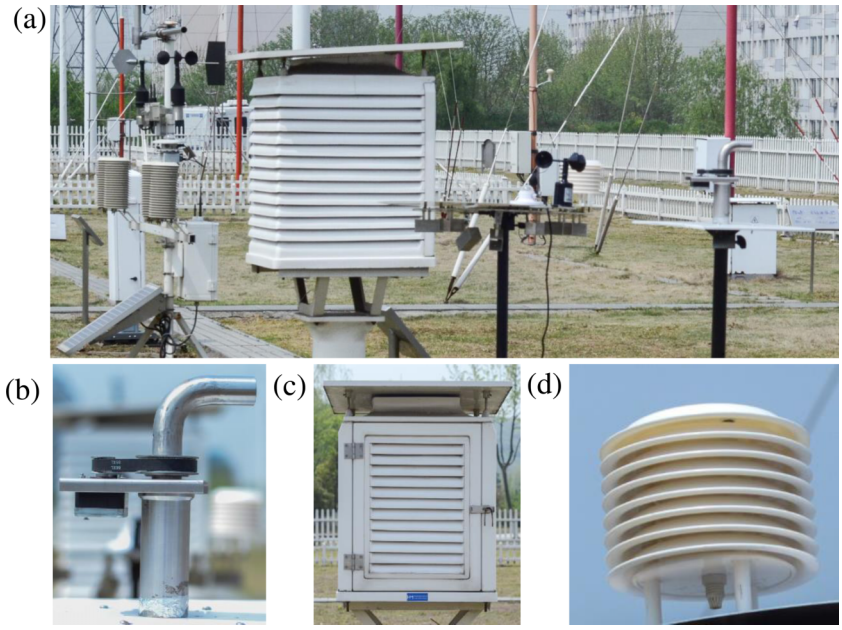


FIG. 4. Photos of experimental setup. (a) is the entire the experimental field. (b)–(d) are the aspirated temperature measurement platform, the thermometer screen, and the naturally ventilated radiation shield, respectively.

The correction equation is obtained by fitting the results shown in Fig. 3,

$$\Delta T = \frac{p_1 + p_2 I + p_3 H + p_4 H^2}{1 + p_5 I + p_6 H + p_7 H^2 + p_8 H^3}, \tag{1}$$

where $p_1 = -0.0003$, $p_2 = 4.2074$, $p_3 = 0.0001$, $p_4 = -1.0901$, $p_5 = 1.293$, $p_6 = -0.1343$, $p_7 = 0.0145$, and $p_8 = -0.0012$. $I$ and $H$ are solar radiation intensity and altitude, respectively.

When the measurement results of the solar radiation intensity and the altitude are plugged into Eq. (1), the radiation error can be obtained. So the observed data of the aspirated temperature measurement platform can be modified, and the temperature measurement accuracy can be improved.

## III. EXPERIMENTAL DEVICE STRUCTURES

The CFD modeling result of the aspirated temperature measurement platform shows that the radiation error diminishes with increasing airflow velocity. However, the power demand increases with increasing airflow velocity. According to the CFD modeling results, if the airflow velocity is 20 m/s, the radiation error is less than 0.05 °C, when the intensity of solar radiation is as large as 1200 W/m$^2$. Therefore, we chose 20 m/s as an upper limit for airflow velocity in our manuscript. When the solar radiation intensity is less than 1000 W/m$^2$, we set the airflow velocity to 8 m/s, because the 8 m/s air flow can allow the radiation error of less than 0.05 °C to be achieved, under this relatively low solar radiation intensity. When the solar radiation intensity is larger than 1000 W/m$^2$, or when the altitude of the weather station is above 2 km, the airflow velocity of 20 m/s is recommended.

In order to verify the actual performance of the aspirated temperature measurement platform and Eq. (1), a number of comparisons have been performed. A Kipp and Zonen CM 21 pyranometer is used to achieve relatively accurate solar radiation intensity (Fig. 4).

## IV. ANALYSIS OF EXPERIMENT RESULTS

Sunny days are chosen to implement the atmospheric temperature observation experiments in the field at Nanjing University of Information Science and Technology Site (32.12°N, 118.42°E, elevation 22 m).

The average radiation errors of the temperature sensors in the thermometer screen and the naturally ventilated radiation shield are 0.25 °C and 0.44 °C, respectively. In contrast, the radiation error of the aspirated temperature measurement platform is as low as 0.05 °C. This aspirated platform allows the radiation error to be reduced by approximately 88.6% compared to the naturally ventilated radiation shield, and allows the error to be reduced by a percentage of approximately 80% compared to the thermometer screen (Fig. 5).

The accuracy of Eq. (1) can be evaluated by using the root mean square error (RMSE) and the mean absolute error (MAE) in (2) and (3), respectively,

$$RMSE = \sqrt{\frac{\sum_{i=1}^{n} (y_{est} - y_{obs})^2}{n}}, \tag{2}$$

$$MAE = \frac{\sum_{i=1}^{n} |y_{est} - y_{obs}|}{n}, \tag{3}$$

where $y_{est}$ is the corrected value from Eq. (1), $y_{obs}$ is the experimental value, and $n$ is the total number of samplings.

From (2) and (3), the MAE and the RMSE between the corrected results and the experimental results are 0.032 °C and 0.036 °C, respectively. It is clear that the difference between these results is a few orders of magnitudes smaller than the

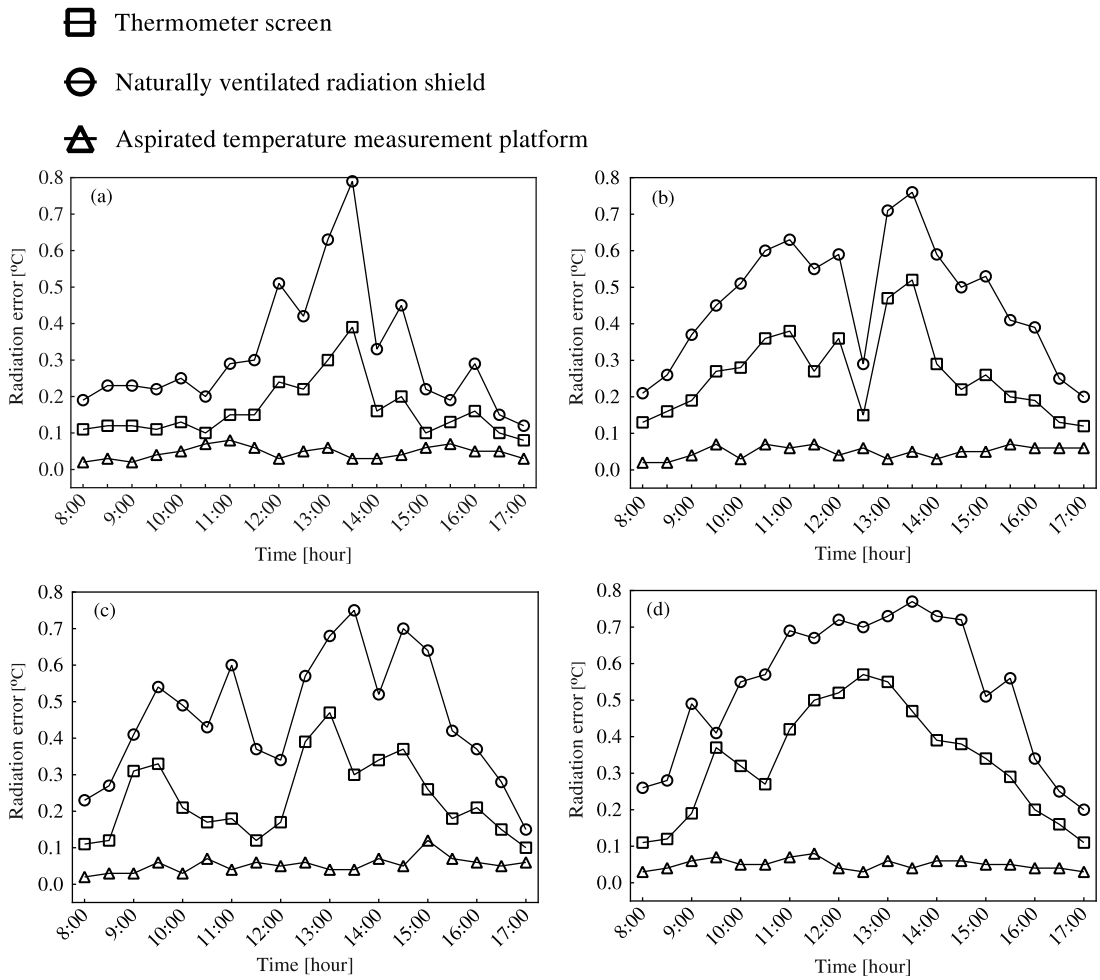


FIG. 5. Comparisons of radiation errors at different times. (a) 9 January 2016; (b) 19 January 2016; (c) 24 January 2016; and (d) 25 January 2016.

radiation errors of traditional naturally ventilated radiation shield and thermometer screen.

## V. CONCLUSIONS

In this paper, an aspirated temperature measurement platform is designed and constructed for obtaining high precision surface temperature measurement results. Numerical calculations have been performed using a CFD method under the conditions of various solar radiation intensities and altitudes. We achieve the correction equation of radiation error by fitting the CFD results employing a GA method. The aspirated temperature measurement platform, the temperature sensors in a naturally ventilated radiation shield and the temperature sensor in a thermometer screen are characterized in one site to conduct surface temperature comparison experiments. The following conclusions may be obtained:

(1) The radiation error increases with the solar radiation intensity, and increases with the increase of altitude.
(2) Compared to the radiation errors of the naturally ventilated radiation shield and the thermometer screen, the radiation error of the aspirated temperature measurement platform is 1–2 orders of magnitude lower.

## ACKNOWLEDGMENTS

This work was supported by the Special Scientific Research Fund of Meteorological Public Welfare Profession of China (Grant Nos. GYHY200906037 and GYHY20130-6079), the National Natural Science Foundation of China (Grant No. 41275042), and the Priority Academic Program Development of Jiangsu Higher Education Institutions (Grant No. PAPD-II).

[1]G. Hans, T. Peter, C. Bo, and J. K. Nielsen, Geophys. Res. Lett. **42**(2), 510, doi:10.1002/2014gl062596 (2015).
[2]J. R. Toggweiler and R. Joellen, Nature **451**(7176), 286 (2008).
[3]Z. A. Holden, J. T. Abatzoglou, C. H. Luce, and L. S. Baggett, Agric. For. Meteorol. **151**(8), 1066 (2011).
[4]J. Balanya, J. M. Oller, R. B. Huey, G. W. Gilchrist, and L. Serra, Science **313**(5794), 1773 (2006).
[5]M. E. Dillon, W. George, and R. B. Huey, Nature **467**(7316), 704 (2010).
[6]A. Haines, A. J. Mcmichael, S. Kovats, and M. Saunders, BMJ Clin. Res. **316**(7143), 1530 (1998).
[7]R. G. Harrison, Q. J. R. Meteorol. Soc. **137**(655), 402 (2011).
[8]R. G. Harrison and C. R. Wood, Q. J. R. Meteorol. Soc. **138**(665), 1114 (2012).
[9]X. Lin, K. G. Hubbard, and G. E. Meyer, J. Atmos. Oceanic Technol. **18**(3), 329 (2010).
[10]S. J. Richardson, F. V. Brock, S. R. Semmer, and C. Jirak, J. Atmos. Oceanic Technol. **16**(11), 1862 (1999).
[11]X. Lin, K. G. Hubbard, and E. A. Walter-Shea, Trans. ASAE **44**(5), 1299 (2001).

[12]M. Fuchs and C. B. Tanner, J. Appl. Meteorol. **4**(4), 544 (1965).
[13]K. G. Hubbard, X. Lin, and E. A. Walter-Shea, J. Atmos. Oceanic Technol. **18**(6), 851 (2001).
[14]S. P. Anderson and M. F. Baumgartner, J. Atmos. Oceanic Technol. **15**(15), 157 (1998).
[15]R. Nakamura and L. Mahrt, J. Atmos. Oceanic Technol. **22**(7), 1046 (2005).
[16]M. Mauder, R. L. Desjardins, Z. Gao, and R. V. Haarlem, J. Atmos. Oceanic Technol. **25**(11), 2145 (2008).
[17]K. G. Hubbard and X. Lin, Geophys. Res. Lett. **29**(10), 67, doi:10.1029/2001GL013191 (2002).
[18]J. A. Hubbart, J. Nat. Environ. Sci. **2**(2), 9 (2011).
[19]M. C. Perry, M. J. Prior, and D. E. Parker, Int. J. Climatol. **27**(2), 267 (2007).
[20]E. Erell, V. Leal, and E. Maldonado, Boundary-Layer Meteorol. **114**(1), 205 (2005).
[21]C. Georges and G. Kaser, J. Geophys. Res. **107**(D24), ACL 15-1, doi:10.1029/2002jd002155 (2010).
[22]G. Lopardo, F. Bertiglia, S. Curci, G. Roggero, and A. Merlone, Int. J. Climatol. **34**(4), 1297 (2014).
[23]C. K. Thomas and A. R. Smoot, J. Atmos. Oceanic Technol. **30**(30), 526 (2013).
[24]R. G. Quayle, D. R. Easterling, T. R. Karl, and P. Y. Hughes, Bull. Am. Meteorol. Soc. **72**(11), 1718 (1991).
[25]F. V. Brock, K. C. Crawford, R. L. Elliott, G. W. Cuperus, S. J. Stadler, H. L. Johnson, and M. D. Eilts, J. Atmos. Oceanic Technol. **12**(12), 5 (1995).
[26]V. Raghavan, S. E. Whitney, R. J. Ebmeier, N. V. Padhye, M. Nelson, H. J. Viljoen, and G. Gogos, Rev. Sci. Instrum. **77**(9), 094301 (2006).
[27]H. Liu, X. Wu, and M. Tan, J. Theor. App. Mech-Pol. **51**(3), 649 (2013).
[28]R. Kurzeja, Boundary-Layer Meteorol. **134**(1), 181 (2010).
[29]S. J. Richardson, J. Atmos. Oceanic Technol. **12**(4), 951 (1995).